Theor Chem Acc (2011) 130:353–359
DOI 10.1007/s00214-011-0990-0

REGULAR ARTICLE

Negative rectification and negative differential resistance in nanoscale single-walled carbon nanotube *p-n* junctions

Lili Yu · Xin Yan · Hong Li · Rui Qin · Guangfu Luo · Chengyong Xu · Jiaxin Zheng · Qihang Liu · Jing Lu · Zhengxiang Gao · Xuefeng Wang

Received: 31 March 2011 / Accepted: 30 June 2011 / Published online: 19 July 2011

Abstract We investigate the transport properties of few-nm-long single-walled carbon nanotube (SWCNT) *p-n* junctions for the first time by using *ab initio* quantum transport calculations. Unlike the previously reported few-μm-long SWCNT *p-n* junctions, which rectify positively, all the investigated ultrashort SWCNT *p-n* junctions show negative rectification effect, accompanied by negative differential resistance.

Keywords Single-walled carbon nanotube · *p-n* junctions · Rectification · Negative differential resistance

Dedicated to Professor Shigeru Nagase on the occasion of his 65th birthday and published as part of the Nagase Festschrift Issue.

Electronic supplementary material The online version of this article (doi:10.1007/s00214-011-0990-0) contains supplementary material, which is available to authorized users.

L. Yu · X. Yan · H. Li · R. Qin · G. Luo · C. Xu · J. Zheng · Q. Liu · J. Lu (✉) · Z. Gao
State Key Laboratory of Mesoscopic Physics and Department of Physics, Peking University, Beijing 100871, People's Republic of China
e-mail: jinglu@pku.edu.cn

J. Zheng
Academy for Advanced Interdisciplinary Studies, Peking University, Beijing 100871, People's Republic of China

X. Wang
Department of Physics, Soochow University, Suzhou 215006, People's Republic of China

1 Introduction

Scaling down of the characteristic dimensions of conventional Si-based optic and electronic devices have become an imperative need, on account of the rising technical demands of modern information society such as high-capacity performance, high-speed capability, high degree of integration, and low-power consumption [1, 2]. However, the miniaturization of traditional Si-based electronic devices is approaching the physical and geometrical limits [3]. On the other hand, single-walled carbon nanotubes (SWCNTs) [4, 5] have attracted a great deal of attentions as a counterpart of silicon in nanoscale in the field of semiconductor devices because of its high carrier mobility, long mean-free-paths of carrier, large aspect ratios (length to diameter), large current density, and flexibility to fabrication [6–15].

The *p-n* junction, which is characterized by rectification, in particular, is one of the fundamental building blocks of electronic circuits for all modern semiconductor devices [16, 17]. When it is heavily doped, it forms Esaki diode and shows negative differential resistance (NDR) [18]. Recently, amounts of efforts have been made to construct *p-n* junctions from semiconducting SWCNTs [19–26]. By covering the left part of a SWCNT with methylmethacrylate (PMMA) layer and then adsorbing potassium atoms onto the surface of the right part, Zhou et al. [20] successfully realized a *p-n* junction with a length of 3.5 μm. This SWCNT *p-n* junction shows rectifying characteristics with typical rectification ratio of 2 or NDR under different gate voltages. Later, air-stable, high-quality (the rectification ratio is about 10^3) and low-leakage SWCNT *p-n* junction with a length of 20 μm was fabricated by Shim with simple photopatterned polymer layers [24]. Recently, Kato et al. [26] utilized controllable plasma ion

irradiation technique to encapsulate Cs/I or Cs/C_{60} inside SWCNTs and obtained air-stable *p-n* junction structures of Cs/I@SWCNTs and Cs/C_{60}@SWCNTs with a length of 1 μm and a maximum rectification ratio between 10^3 and 10^4. To our knowledge, all these experimentally achieved SWCNT *p-n* junctions are in the micro-length scale which is about ten times larger than current silicon transistors and always rectify in the positive direction. Namely, it is easier for current to flow from the *p* region to the *n* region. Besides, in most cases, there is no NDR effect in these SWCNT *p-n* junctions.

On the other hand, amounts of theoretical and experimental research have been done on the donor-insulator-acceptor (DσA) molecular diodes (also called the Aviram–Ratner molecular diodes) since it was proposed by Aviram and Ratner in 1974 theoretically [27–34]. In this DσA model, the donor (D) and acceptor (A) wires connect to external reservoirs, respectively, and the σ bonds between them introduce an effective barrier to block the electron from transferring through. Because of the lower oxidation potential and higher energy level of the D wire, electrons and holes are injected into the A and D segments, respectively, and subsequent annihilation happens in this system. Consequently, current will flow easier from D to A region; thus, the Aviram–Ratner molecular diodes rectify in the negative direction.

What will happen if the length of a SWCNT *p-n* junction is reduced to molecular size? Several fundamental and intriguing questions arise: (1) Does the few-nm-long SWCNT *p-n* junction still rectify? (2) Which direction will the rectification be in? (3) Are NDR effects available in this device? In this article, we investigate the transport properties of few-nm-long SWCNT *p-n* junctions by using density functional theory (DFT) combined with non-equilibrium Green's function (NEGF) method. Contrary to the micro-length-scale SWCNT *p-n* junctions, negative rectification effects are observed in all these studied ultrashort SWCNT *p-n* junctions, accompanied by NDR effects.

2 Model and method

To fabricate SWCNT *p-n* junctions, nitrogen (N) and boron (B) atoms are doped to substitute for two carbon atoms (as shown in Fig. 1a), converting the two ends of the semiconducting (7, 0) SWCNT to *n*-type and *p*-type, respectively. We also dope the interior of the SWCNT with potassium (K) and I iodine (I) along the axis of the tube, serving as donor and acceptor, respectively (as shown in Fig. 1b). It has been tested that the transmission spectrum and current are not sensitive to small changes in the position of the dopants. Here, we use B-SWCNT-N(*m*) and I-SWCNT-K(*m*) to denote different types of SWCNT *p-n* junctions, where *m* represents the number of unit cells of the SWCNT along the transport direction. We have chosen *m* to be 6, 8, 9, 10, 11, 12, and 16 and the corresponding lengths of the SWCNT *p-n* junctions range from 2.5 to 7.0 nm. The two-probe device is fabricated to calculate the transport property. It is divided into left electrode, extended molecule, and right electrode three parts, as shown in Fig. 1a. The extended molecule consists of the SWCNT *p-n* junction and four surface layers of two lithium (Li) electrodes. Our test shows that longer surface layers would not significantly affect the transport properties, which means four surface layers provide sufficient screening to keep the electrode bulk-like. In our model, as many as 500 atoms are involved, and we use the simple Li electrodes to save computational cost, which have already been used in some other transport calculations [35, 36]. The two homogeneous semi-infinite metal electrodes are quasi-one-dimensional and represented by a 3×3 unit cell with Li (100) as surface. The SWCNT–metal separation is 2.3 Å, providing a strong coupling at the interface. No optimization is performed for the SWCNT–metal contact to maintain a symmetric current about the bias, otherwise the effects of the donor and acceptor doping will be overwhelmed by the asymmetric SWCNT–metal contact.

The transport properties are calculated by the Atomistix Toolkit 2008.10 code, which is based on the combination of DFT with NEGF method [37–39]. In our calculation, the Perdew-Burke-Ernzerhof (PBE) form of the generalized gradient approximation (GGA) [40] for exchange–correlation functional is used. Single-ζ function is used as basis set for the valence orbitals of each atom. Each ion plus its core electrons are described by norm-conserving pseudo-potentials [41]. The mesh cutoff of electron density is chosen as 150 Ry, and a Monkhorst–Pack $1 \times 1 \times 500$ *k*-mesh is used [42] to achieve a balance between calculation efficiency and accuracy. The electron temperature is set to 300 K, and the convergence criterion for the total energy is 10^{-5} Ry. The current is calculated using the Landauer-Büttiker formula [43],

$$I(V) = \frac{2e}{h} \int_{-\infty}^{+\infty} \{T(E,V)[f_{\mathrm{L}}(E-\mu_{\mathrm{L}}) - f_{\mathrm{R}}(E-\mu_{\mathrm{R}})]\}\mathrm{d}E \quad (1)$$

where $T(E,V)$ is the transmission probability, $f_{\mathrm{L/R}}$ the Fermi–Dirac distribution function for the left (L)/right (R) electrode, and $\mu_{\mathrm{L}}/\mu_{\mathrm{R}}$ the electrochemical potential of the left (L)/right (R) electrode.

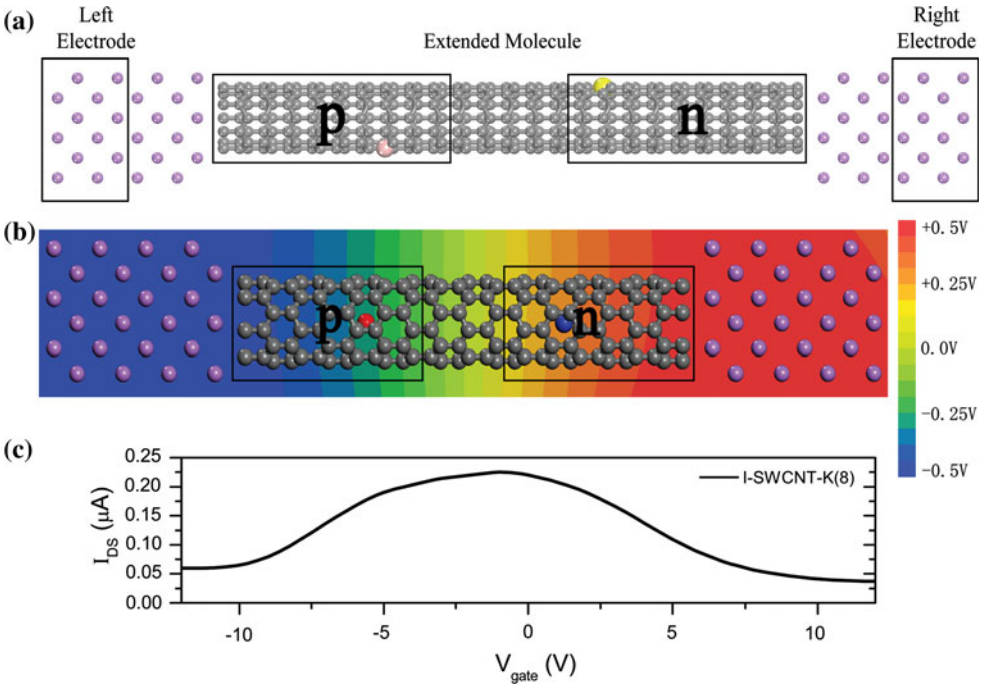

Fig. 1 Two-probe model of the (7, 0) SWCNT *p-n* junction connected to Li electrode: **a** Substitutional doping of B and N as acceptor and donor, respectively, in the SWCNT with 12 unit cells. **b** Interior doping of I and K atoms in the tube axis as acceptor and donor, respectively, in the SWCNT with 8 unit cells. In **b**, the large voltage drop in the central region of the *p-n* junction is apparent from the shown voltage contour at the bias of 1 V. *Grey ball*: C; *purple ball*: Li; *red ball*: I; *blue ball*: K; *pink ball*: B; *yellow ball*: N. **c** $I_{DS}-V_{gate}$ characteristics of the I-SWCNT-K(8) junction under a source-drain bias voltage of $V_{DS} = 0.01$ V. The symmetrical current hump about the gate voltage is unique to *p-n* junctions [20, 26]

3 Result and discussion

The voltage drop at $V_{bias} = 1.0$ V of the K-SWCNT-I(8) model is shown in Fig. 1b. It is clearly shown that the effective potential drops non-linearly in different parts of the device. The homogeneous voltage drop in the electrode and surface layers demonstrates sufficient screening of the surface layers. Little voltage drop is detected at the Li–C atom interfaces, which means small resistance at the metal–SWCNT interface, in agreement with the previous study that the localized hybridization between the electron states of carbon and metal atoms lowers the potential barrier at the metal–SWCNT interface [44]. A large voltage drop occurs in the central region of the *p-n* junction, indicative of formation of a barrier region between the *p* region and *n* region. In order to confirm the formation of the SWCNT *p-n* junctions, the transfer character of the I-SWCNT-K(8) junction is investigated and shown in Fig. 1c. A remarkable symmetrical hump structure about the gate voltage is observed, which is unique to *p-n* junctions [20, 26] and also observed in few-μm-long SWCNT *p-n* junctions [26].

The I–V_{bias} characteristics of a pure SWCNT with length of 8 unit cells and 8 SWCNT *p-n* junctions are plotted in Fig. 2. The I–V_{bias} curve of the pure ultrashort SWCNT is symmetric about V_{bias}, non-linear, and has some steps. Experimentally, the I–V_{bias} curve of a few-nm-long pure SWCNT [45, 46] is linear at lower bias and saturates at higher bias. We attribute this difference to a substantial difference in the contact way. In the experiment, the electrodes are deposited on the SWCNTs and form weak non-covalent contact on the sidewall of SWCNTs. However, in our two-probe model, the metal electrodes form strong covalent contact at the ends of the SWCNTs. The transport property is sensitive to the contact way, and different contacts lead to the different I–V_{bias} curves. Remarkably, negative rectification is observed in all checked SWCNT *p-n* junctions. Apparently, the negative rectification is ascribed to the donor and acceptor doping on the semiconducting SWCNT rather than an asymmetric contact between the nanotubes and source and drain electrodes as reported in some previous studies [25]. The negative rectification in few-nm-long SWCNT *p-n* junctions is contrary to a positive rectification in few-μm-long SWCNT *p-n* junctions but consistent with that in typical Aviram–Ratner molecular diodes. Therefore, the rectification direction of SWCNT *p-n* junctions strongly depends on their size. The rectification ratio (RR) is defined as $RR = |I_-/I_+|$, where I_+ and I_- are the currents under the positive and negative bias, respectively. Generally, at small bias of lower than 0.4 V, there are no obvious rectifications, and with the increasing of the absolute value of the bias voltages, RRs first increase to 4.0–17.6, then decrease, and finally all these *p-n* junctions keep constant RRs between 1.5 and 2.5 from $V_{bias} = 1.2$–2 V. The RR reaches the largest value of 17.6 in the B-SWCNT-N(12) junction at $V_{bias} = 0.8$ V.

In addition to negative rectification effect, NDR effects are observed in all these checked SWCNT *p-n* junctions in both positive and negative bias voltages. By contrast, NDR only exists under positive bias voltages in Esaki diodes. The current drops are generally several μA with the largest

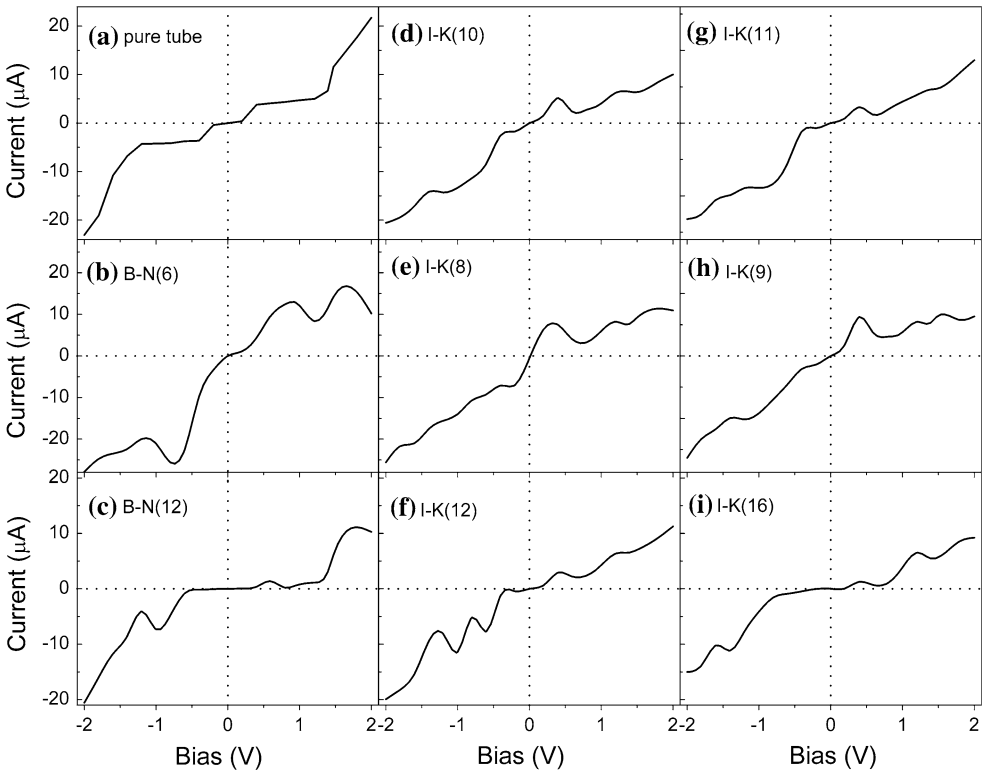

Fig. 2 I–V_{bias} characteristics of **a** a pure (7, 0) SWCNT with a length of 8 unit cells, **b**, **c** the B-SWCNT-N(m) ($m = 6$ and 12) and **d**–**i** the I-SWCNT-K(m) ($m = 8$, 9, 10, 11, 12, and 16) junctions. Rectification in negative direction and negative differential resistance effects can be observed from these curves

value of 4.7 μA in both the B-SWCNT-N(6) (Fig. 2d) and the I-SWCNT-K(9) junctions (Fig. 2f). Such current drops are comparable with those in other SWCNT-based NDR devices [47–49]. In all the I-SWCNT-K(m) junctions, the current firstly begin to drop from $V_{\text{bias}} = 0.4$ V (NDR effect). The largest peak-to-valley ratio (PVR) of current is 5 in the checked p-n junctions (the B-SWCNT-I(12) junction).

Figure 3 shows the contours plot of the transmission spectra of the pure SWCNT(8) and I-SWCNT-K(8) as a function of the bias voltage. The transmission spectra of the pure SWCNT(8) are symmetrical about the positive and negative bias voltage, a result in agreement with no rectification effect in pure tube. However, the transmission spectra under negative bias of the I-SWCNT-K(8) are apparently stronger than those under positive bias, a result consistent with a larger current under negative bias in the I-SWCNT-K(8) junction (Current is an integration of the transmission coefficients within the bias window). There is a transmission peak near $E-E_f = 0.1$ eV, and it disappears at bias of larger than 0.4 V, and this is responsible for the first current drop from $V_{\text{bias}} = 0.4$ V. Consequently, the first NDR peak appears.

As an effort to deeply understand the origin of the negative rectification, we calculate both the molecular projected self-consistent Hamiltonians (MPSHs, namely the molecular levels under certain chemical environment) (shown in the supporting information) and projected density of states (PDOS) of the p and n regions. The correlation between the PDOSs of the p and n regions and the transmission spectra is significantly better than that between the MPSHs of p and n regions and the transmission spectra. The cause lies in the fact that the interaction between the SWCNT (scattering region) and metal electrodes and that between the p and n regions in this case are so strong that the MPSHs make less sense. Therefore, we adopt the PDOSs to analyze the transport feature of nanoscale SWCNT p-n junctions. Actually, PDOSs have been adopted by other researchers to successfully explain the NDR effects in graphene nanoribbon [50]. We show the transmission spectra and PDOSs at $V_{\text{bias}} = 0$ (middle panel in Fig. 4), 1.2 (right panel in Fig. 4) and -1.2 V (left panel in Fig. 4) of the p and n regions for the I-SWCNT-K(8) junction. The zero-bias transmission spectra and PDOSs of the pure SWCNT are shown in red dotted line for the purpose of comparison. If we consider the phonon scattering, the above transmission spectra would be much smoother. Unfortunately, such a function is not introduced in the present Atomistix package. The relation between the transmission coefficient $T(E)$ and PDOSs of the p and n regions can be described empirically by

$$T(E) = \text{PDOS}(p\,\text{region}) \times \text{PDOS}(n\,\text{region}) \times \lambda(E) \quad (2)$$

where $\lambda(E)$ is a coupling strength.

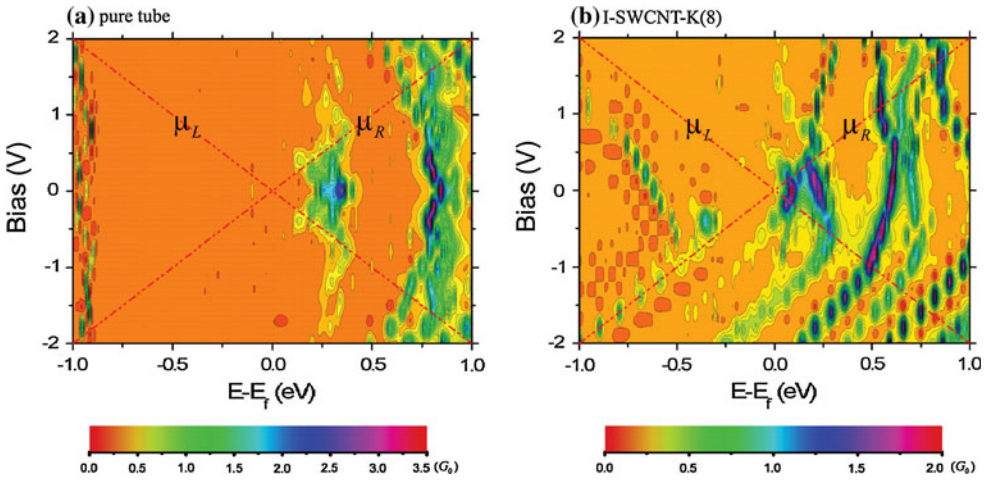

Fig. 3 Contour plots of the transmission spectra as a function of bias voltage. **a** Symmetric contour about positive and negative bias of the pure (7, 0) SWCNT. **b** Asymmetric contour about positive and negative bias of the I-SWCNT-K(8) junction. The transmission window for the current integration is demonstrated as the region between the *red* crosses of $\mu_L(V_{bias}) = \mu_L(0) - eV_{bias}/2$ and $\mu_R(V_{bias}) = \mu_R(0) + eV_{bias}/2$

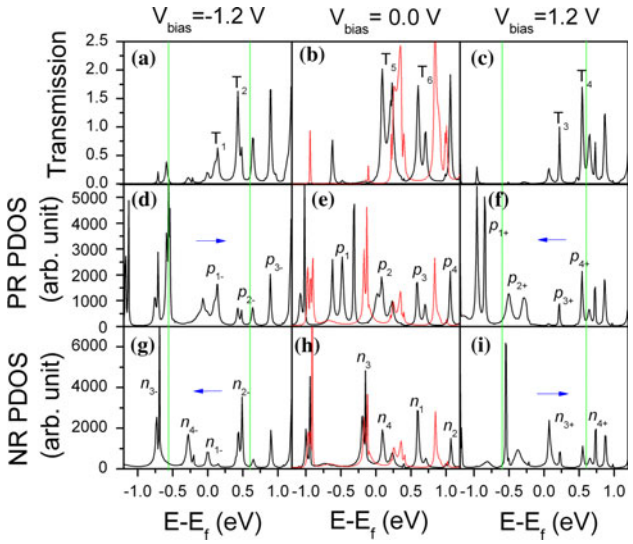

Fig. 4 **a–c** Transmission spectra and PDOSs of the *p* region (PR PDOS) (**d–f**) and *n* region (PN PDOS) (**g–i**) of the I-SWCNT-K(8) junction (*black line*) at bias voltages of −1.2, 0.0, and 1.2 V, respectively. The zero-bias transmission spectrum and PDOSs of the pure (7, 0) tube is also shown in *red dotted line*. The *green doted vertical line* indicates the bias window. Some major peaks in the transmission spectrum, PR PDOS, and NR PDOS are labeled

The two large double-peaks at $E = 0.17$ (T_5 peak) and 0.65 (T_6 peak) eV under zero bias of the I-SWCNT-K(8) junction are ascribed to a resonant tunneling between the two PDOS double-peaks in the *p* region (p_2 and p_3 peaks) and the two PDOS double-peaks in the *n* region (n_4 and n_1 peaks) at the same energy. The PDOSs at the *p* and *n* regions are nearly identical for the pure SWCNT, and the I–V_{bias} characteristic is symmetric. The PDOSs at the *p* and *n* regions become asymmetric in the I-SWCNT-K(8) junction, causing an asymmetric I–V_{bias} characteristic. At positive/negative bias, the PDOS peaks in the *p/n* and *n/p* regions for the I-SWCNT-K(8) junction move roughly linearly with the bias toward the lower and higher energy direction, respectively, because they feel opposite electrostatic fields. But the shapes of the PDOS peaks can be changed greatly by the bias. In Fig. 4b, c, the PDOS peaks labeled as p_{1-}/n_{1-}, p_{2-}/n_{2-}, p_{3+}/n_{3+}, and p_{4+}/n_{4+} under bias voltage of −1.2 V/1.2 V originate from the PDOS peaks labeled as p_1/n_1, p_2/n_2, p_3/n_3, and p_4/n_4 at zero bias voltage, respectively. At $V_{bias} = -1.2$ V, two wider PDOS peaks at 0.1 and 0.43 V in the *p* (p_{1-} and p_{2-}) region within the bias window resonate with those in the *n* (n_{1-} and n_{2-}) region, forming two wider transmission peaks (T_1 and T_2). At $V_{bias} = 1.2$ V, two shaper PDOS peaks at 0.23 and 0.55 V in the *p* (p_{3+} and p_{4+}) and *n* (n_{3+} and n_{4+}) regions resonate within the bias window, forming two shaper transmission peaks (T_3 and T_4). The currents are an integral of the transmission coefficients within the bias window, and thus, the current at $V_{bias} = -1.2$ V is larger than that at $V_{bias} = 1.2$ V. The larger width of the p_1 and p_2 peaks than the p_3 and p_4 peaks are responsible for the larger width of the p_{1-} and p_{2-} peaks than the p_{3+} and p_{4+} peaks and thus responsible for the negative rectification behavior.

The positive rectification in the traditional *p-n* junction can be understood in terms of the band structures of *p*- and *n*-doped semiconductors well separated by a barrier (space carrier region). The SWNT *p-n* junction with μm length is still can be characterized by the traditional *p-n* junction and has a positive rectification. However, the barrier is too short, and the interaction of the *p* region and *n* region is so strong that the band concept of the traditional *p-n* junction is completely invalidated as the length of the SWNT *p-n* junction is reduced to a few nm. In this case, the rectification direction depends on the complex coupling of the *p* region and *n* region and can no longer be predicted by a simple band model and negative rectification becomes possible.

To demonstrate the electron spatial distribution when a resonant tunneling happens, we separately calculated eigenstates of MPSHs of the *p* and *n* regions. The

isosurfaces of the eigenstates in the p and n regions at $E-E_f = 0.43/0.55$ eV (transmission peak T_2/T_4) are shown in Fig. 5a, c. The positive/negative part of the wave function of the p region corresponds to positive/negative part of that of the n region, and this sign match favors large transmission. The transmission eigenchannels of the T_2/T_4 peaks with eigenvalues of 1.6 and 1.7, respectively, (compared with an eigenvalue of 2 in perfect transmission) are displayed in Fig. 5b and d, respectively. These channels extended to the whole device, which means that the incoming wave function is scattered slightly and it is easy for the electrons to pass through the whole SWCNT p-n junction when resonant tunneling happens between the p and n regions.

Till now, no nanoscale SWCNT p-n junctions have been realized in experiment. However, nanoscale SWCNT field effect transistors (FET) [45, 46] and various macroscale SWCNT p-n junctions [20, 24, 26] have been already realized. Here, we propose several ways to realize nanoscale SWCNT p-n junctions. (1) Thanks to the development of lithographic techniques, it is possible to construct dual-gate in the nanoscale SWCNT channel to create n- and p-doped regions by separate gate [51, 52]. (2) Nanoscale SWCNT p-n junction could be fabricated by further downsizing the previously reported macroscale SWCNT p-n junctions [20, 24, 26] constructed by polymer-induced doping, chemical treatment by gas exposure, plasma ion irradiation. We expect that with the development of fabrication techniques, the nanoscale SWCNT p-n junctions could be brought out soon.

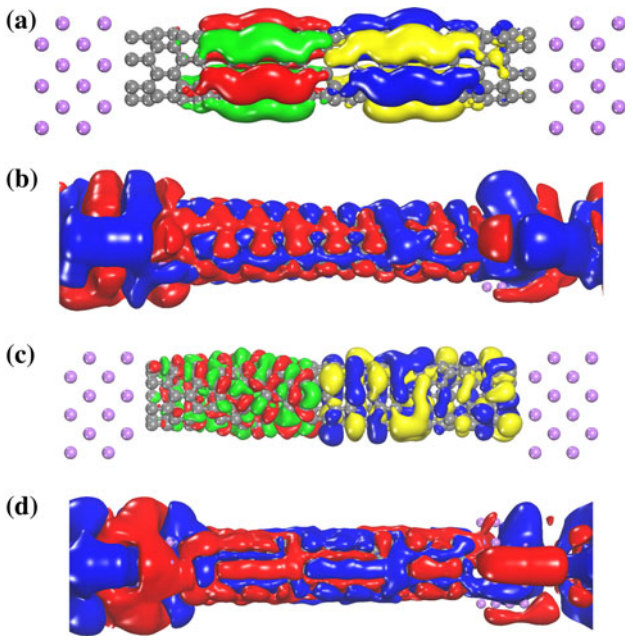

Fig. 5 Isosurfaces of the eigenstate of the MPSH (**a**) and the first transmission eigenchannel (**b**) of the I-SWCNT-K(8) junction at $E-E_f = 0.43$ eV (transmission peak T_2 in Fig. 4a) under bias voltage of -1.2 V. *Left*/*right* half of the isosurface in **a** is the 192th/190th orbital of the energy spectrum of MPSH (corresponding to the p_{2-}/n_{2-} peak in Fig. 4d, g) of the *p*/*n* region. Isosurfaces of the eigenstate of the MPSH (**c**) and the first transmission eigenchannel (**d**) of the I-SWCNT-K(8) junction at $E-E_f = 0.55$ eV (transmission peak T_4 in Fig. 4c) under bias voltage of 1.2 V. *Left*/*right* half of the isosurface in (**c**) is the 194th/189th orbital of the energy spectrum of MPSH (corresponding to p_{4+}/n_{4+} in Fig. 4d, g) of the *p*/*n* region, respectively. In **a** and **c**, the isovalue is 0.025 a.u., and *red*/*blue* and *green*/*yellow* indicate the positive and negative signs of the wave functions, respectively. In **b** and **d**, the isovalue is 0.005 a.u., and *red* and *blue* are used to indicate the positive and negative signs of the wave functions, respectively

4 Conclusion

We calculate the transport properties of several few-nm-long SWCNT p-n junctions. Contrary to the micro-length-scale SWCNT p-n junctions, negative rectification effects are observed in all these studied ultrashort SWCNT p-n junctions accompanied by the NDR effects. Our results show that when the size of a SWCNT p-n junction is minimized to nanoscale, the rectification direction may see a dramatic change. This study is expected to promote the realization of SWCNT p-n junctions in the nanometer scale and observation of Aviram and Ratner diode behavior in them.

5 Supporting information available

Molecular projected self-consistent Hamiltonians of the p and n regions and transmission spectrum of the I-SWCNT-K(8) junction at zero bias.

Acknowledgments This work was supported by the NSFC (Grants Nos. 10774003, 90626223, and 20731162012), National 973 Projects (Grant No. 2007CB936200, MOST of China), Fundamental Research Funds for the Central Universities, Program for New Century Excellent Talents in University of MOE, National Foundation for Fostering Talents of Basic Science (Grant No. J0630311) of China. We thank Prof. Toshiaki Kato for helpful discussion.

References

1. Ellenbogen JC, Love JC (2000) Proc IEEE 88:386
2. Cao Y, Steigerwald ML, Nuckolls C, Guo XF (2010) Adv Mater 22:20
3. Yan QM, Huang B, Yu J, Zheng FW, Zang J, Wu J, Gu BL, Liu F, Duan WH (2007) Nano Lett 7:1469
4. Iijima S (1991) Nature 354:56
5. Iijima S, Ichihashi T (1993) Nature 363:603
6. Park H, Zhao J, Lu JP (2006) Nano Lett 6:916
7. Tsuneta T, Lechner L, Hakonen PJ (2007) Phys Rev Lett 98:087002

8. Wei D, Liu Y (2008) Adv Mater 20:2815
9. Zhou W, Bai X, Wang E, Xie S (2009) Adv Mater 21:4565
10. Lee SU, Belosludov RV, Mizuseki H, Kawazoe Y (2009) Small 5:1769
11. Kienle D, Léonard F (2009) Phys Rev Lett 103:026601
12. Kanungo M, Lu H, Malliaras GG, Blanchet GB (2009) Science 323:234
13. Oshima Y, Takenobu T, Yanagi K, Miyata Y, Kataura H, Hata K, Iwasa Y, Nojiri H (2010) Phys Rev Lett 104:016803
14. Wang ZH, Wei J, Morse P, Dash JG, Vilches OE, Cobden DH (2010) Science 327:552
15. Kim S, Janes DB, Mohammadi S, Back J, Shim M (2010) Nanotechnology 21:385203
16. Chang LL, Esaki L, Tsu R (1974) Appl Phys Lett 24:593
17. Shockley W (1976) IEEE Trans Electron Devices 23:597
18. Esaki L (1976) IEEE Trans Electron Devices 23:644
19. Esfarjani K, Farajian AA, Hashi Y, Kawazoe Y (1999) Appl Phys Lett 74:79
20. Zhou C, Kong J, Yenilmez E, Dai H (2000) Science 290:1552
21. Lee JU, Gipp PP, Heller CM (2004) Appl Phys Lett 85:145
22. Li J, Zhang Q, Chan-Park MB (2006) Carbon 44:3087
23. Li YF, Hatakeyama R, Shishido J, Kato T, Kaneko T (2007) Appl Phys Lett 90:173127
24. Abdula D, Shim M (2008) ACS Nano 2:2154
25. Li H, Zhang Q, Marzari N (2008) Nano Lett 8:64
26. Kato T, Hatakeyama R, Shishido J, Oohara W, Tohji K (2009) Appl Phys Lett 95:083109
27. Aviram A, Ratner MA (1974) Chem Phys Lett 29:277
28. Metzger RM (1995) Mater Sci Eng C 3:277
29. Metzger RM (2001) Synth Met 124:107
30. Krzeminski C, Delerue C, Allan G, Vuillaume D, Metzger RM (2001) Phys Rev B 64:085405
31. Stokbro K, Taylor J, Brandbyge M (2003) J Am Chem Soc 125:3674
32. Stadler R, Geskin V, Cornil J (2008) J Phys Condens Matter 20:374105
33. Ford MJ, Hoft RC, McDonagh AM, Cortie MB (2008) J Phys Condens Matter 20:374106
34. He HY, Pandey R, Mallick G, Karna SP (2009) J Phys Chem C 113:1575
35. Ng MF, Shen L, Zhou LP, Yang SW, Tan VBC (2008) Nano Lett 8:3662
36. Wang ZY, Li H, Liu Z, Shi ZJ, Lu J, Suenaga K, Joung SK, Okazaki T, Gu ZN, Zhou J, Gao ZX, Li GP, Sanvito S, Wang EG, Iijima S (2010) J Am Chem Soc 132:13840
37. Taylor J, Guo H, Wang J (2001) Phys Rev B 63:121104
38. Brandbyge M, Mozos JL, Ordejón P, Taylor J, Stokbro K (2002) Phys Rev B 65:165401
39. Stokbro K, Taylor J, Brandbyge M, Ordejón P (2003) Ann NY Acad Sci 1006:212
40. Perdew JP, Burke K, Ernzerhof M (1996) Phys Rev Lett 77:3865
41. Troullier N, Martins JL (1991) Phys Rev B 43:8861
42. Monkhorst HJ, Pack JD (1976) Phys Rev B 13:5188
43. Buttiker M, Imry Y, Landauer R, Pinhas S (1985) Phys Rev B 31:6207
44. Bai P, Li E, Lam KT, Kurniawan O, Koh WS (2008) Nanotechnology 19:115203
45. Javey A, Qi PF, Wang Q, Dai HJ (2004) Proc Natl Acad Sci USA 101:13408
46. Franklin AD, Chen ZH (2010) Nat Nanotechnol 5:858
47. Khoong Hong K, Neaton JB, Young Woo S, Cohen ML, Louie SG (2008) Nano Lett 8:2900
48. Xu Y, Zhang G, Li BW (2008) J Phys Chem B 112:16891
49. Kim WY, Kwon SK, Kim KS (2007) Phys Rev B 76:4
50. Hao R, Li Q, Luo Y, Yang J (2009) Appl Phys Lett 94:173110
51. Williams JR, DiCarlo L, Marcus CM (2007) Science 317:638
52. Chiu HY, Perebeinos V, Lin YM, Avouris P (2010) Nano Lett 10:4634